Characterization of a NE-213 liquid scintillator for neutron flux measurement at JET

Federico Binda
Uppsala University, Sweden

March, 2011

Abstract

The measurment of the total neutron rate from a nuclear fusion reactor is very important in order to calculate the power produced in a plasma. An improvement of a method currently in use at JET will involve the installation of an organic liquid scintillator NE-213 of 1 cm^3 of volume combined with a digital acquisition card.

In this project a first stage of the characterization of the digitizer and of the detector has been performed.

1 Introduction

1.1 Nuclear fusion

Nuclear fusion is a process in which two light nuclei melt together in order to create a heavier, more stable nucleus, with a consequent release of energy. The isotopes that are most commonly considered for fusion reactors are deuterium and tritium, giving the reactions in table 1. Every DT reaction produces one neutron while the DD reaction have another branch, so it gives one neutron every two reactions. Therefore from the number of neutrons released it is possible to calculate the power produced.

These processes can only occur when the two nuclei have enough energy to overcome the Coulomb repulsion, a condition that can be achieved at very high temperatures ($\sim 10^8$K), when matter is in a particular state called plasma.

Plasmas can be handled using special machines called Tokamaks, that generate a magnetic field which can force the plasma to remain in a limited region, exploiting the fact that its particles are ionized.

1.2 JET

JET (Joint European Torus) is a fusion reactor situated near Culham, in the UK. It's tokamak is the largest in the world and the only one capable to handle DT fusion. The neutron detectors installed at JET are: TOFOR (Time Of Flight nutron spectrometer Optimized for high count Rate), that is optimized for DD neutron spectrometry; MPRu (Magnetic Proton Recoil spectrometer upgrade), that is optimized for DT neutron spectrometry, but has been upgraded to provide also data from DD operations; two cameras for neutron emission profile monitoring; fission chambers for total yield monitoring.

Table 1: DD and DT fusion reactions.

Reaction	E_N (MeV)	E_{TOT} (MeV)
$d + d \longrightarrow {}^3He + n$	2.5	3.3
$d + t \longrightarrow {}^4He + n$	14.0	17.6

1.3 Neutron yield measurement at JET

One method in use at JET for neutron yield measurement combines the plasma emission profile provided by the monitor camera with the neutron flux recorded by the MPRu [1]. However the low efficiency of the spectrometer limits the time resolution in trace T and D operations, keeping it at the order of seconds. Because of this a new technique in the flux measurement that can improve the time resolution to the order of milliseconds has been proposed. This involves the use of a cylindrical organic liquid scintillator NE-213 (see fig.1 and tab.2) that can provide a high count rate even in D operations, thereby giving good time resolution.

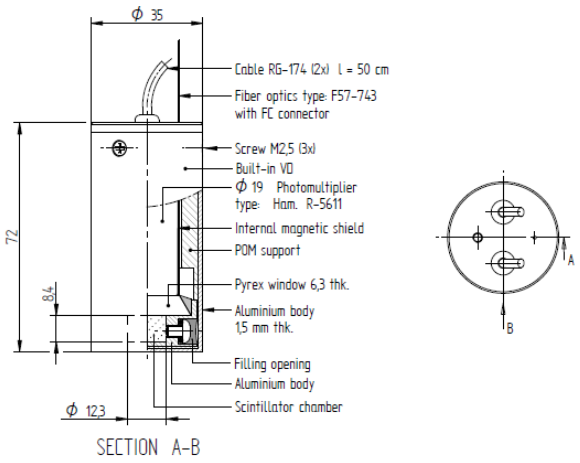

Figure 1: Drawing of the detector. The active area is labelled as 'Scintillator chamber'. There are three cables coming out from the photomultiplier: one is for the signal output, one for the HV input and the thin one is an optical fiber that can be used to send light signals to the PMT from an external source (e.g. a LED pulse generator).

Table 2: NE-213 main features

Chemical compound	Xylene (C_8H_{10})
Density	0.874 g/cm^3
Light output	78% of anthracene
Decay time	3.7 ns
Wavelength of max. emission	425 nm
Height	8.4 mm
Diameter	12.3 mm
Volume	998 mm^3

NE-213 detectors can detect both neutrons and photons in two similar ways that however have a very important difference: neutrons interact with protons while photons undergo Compton scattering on electrons. The molecules of the detector are then excited by these charged particles and successively de-excited by the emission of visible light, that is collected by the photomultiplier tube. This is composed of a plate that converts photons into electrons through the photoelectric effect and a chain of dynodes that multiply the electrons. A potential difference between the dinodes drives the electrons in the tube.

The output of the PMT is a current pulse that can be sent to some acquisition device (the digitizer in this case). The total charge collected gives the information of the energy released by the particle that hit the detector, while the shape of the pulse carries important information about the charged particle that generated it. Indeed electrons produce pulses that decay faster than the ones produced by protons (fig.2), so the use of this kind of detectors allows γ/n pulse shape discrimination.

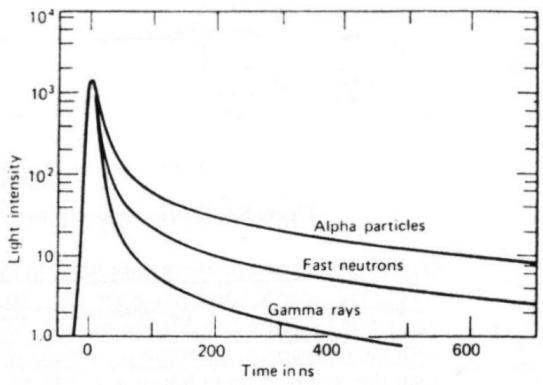

Figure 2: Pulses generated by different particles in an organic scintillator. (from [2]).

The photomultiplier's gain, i.e. the total charge collected at a fixed intensity of the light that reaches the tube, can vary because of many factors (temperature, count rate...). Therefore a gain monitoring system, which involves the use of a ^{22}Na calibration source and a LED pulse generator, will be installed together with the detector. The source will give an absolute reference for gain corrections, but some hours are required to have a satisfactory spectrum, so it can provide only corrections for the long period. The LED generator will produce monoenergetic pulses that can give the necessary information for gain corrections in the short period. It cannot be used for the long term corrections because the LED device itself can be subject to some drifts in the integrated charge spectrum.

2 Energy calibration

As previously stated in 1.3 the total charge collected at from the PMT is proportional to the energy deposited by the incident particle. This charge is distributed in time, so the collected data are pulses that look like figure 3. The total charge can be obtained looking at the area under the pulse, but one must be careful to consider the baseline restoration. The baseline is the current level when no pulse is present (figure 3), and what is important is the amplitude variation with respect to this level. For electrons the area measured is linearly proportional to the energy and the coefficients of this relationship need to be determined experimentally.

Calibration sources emit radiation at fixed and very well known energies, so they can be used as references for the calibration of the detector and acquisition system. If one plots the distribution of the total charge values for many collected pulses (the spectrum), one can locate the signatures in this distribution that correspond to the known energies of the source and find the sought coefficients. In this project gamma sources of ^{22}Na and ^{137}Cs have been used.

It's important to remember that the calibration curve is strongly dependent on the high voltage supply of the PMT, i.e. the gain grows exponentially with the tension:

$$G(V) = Ae^{B \cdot V} \tag{1}$$

2.1 Measurements

The acquisition of ^{22}Na source spectra has been performed with high voltage supply values ranging from -700 V to -900 V with 50 V steps. The integrated charge spectrum (fig.5) should have two "shoulders", corresponding to the Compton edges of the two monoenergetic photons from sodium. However, because of the finite resolution of the detector these shoulders are not exactly located on the Compton edge position. It can be shown [3] that the real position is at 89% of the maximum height of the measured peak.

The resolution function of the detector has been measured (fig.4) fitting the data from ^{22}Na and ^{132}Cs with the function:

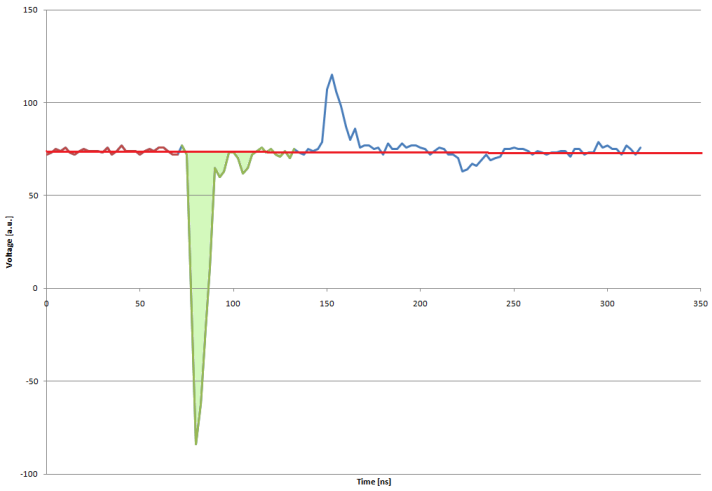

Figure 3: Example of a collected pulse. The red line is the baseline level while the light green is the integrated area.

$$R(E) = \frac{FWHM(E)}{E} = \sqrt{\alpha^2 + \frac{\beta^2}{E} + \frac{\gamma^2}{E^2}} \tag{2}$$

where E is the energy position of the measured peak, while α, β and γ are experimental coefficients respectively related to (α) the position of the scintillation in the detector, (β) the statistical fluctuations and (γ) the noise from both the photomultiplier and the electronic data acquisition devices.

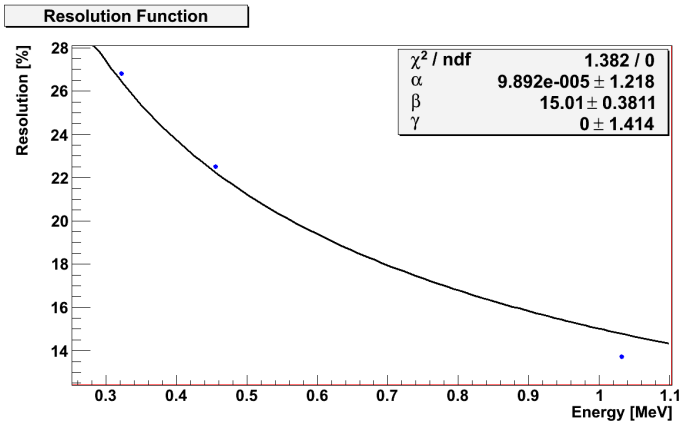

Figure 4: resolution function.

In the measured spectrum of ^{22}Na can be seen that the second peak corresponding to 1.061 MeV is not prominent as it should be. This could be related to the escape of some of the secondary electrons because of the small size of the detector, so that they don't deposit all their energy. A MCNP model has been developed in order to verify this hypotesis. The simulation does not take into account the resolution of the detector, so its outcome must be folded with the resolution function previously obtained. In fact each point of the simulated spectrum is generated as a delta function, while in reality it is a gaussian distribution with a spread that depends on the resolution of the detector at that energy (2). The final distribution obtained has good agreement with the experimental data (fig.5).

In figure 6 the relationship between gain and HV for the 1.061 MeV sodium peak is shown. The experimental data and the fitting function (1) are in good agreement.

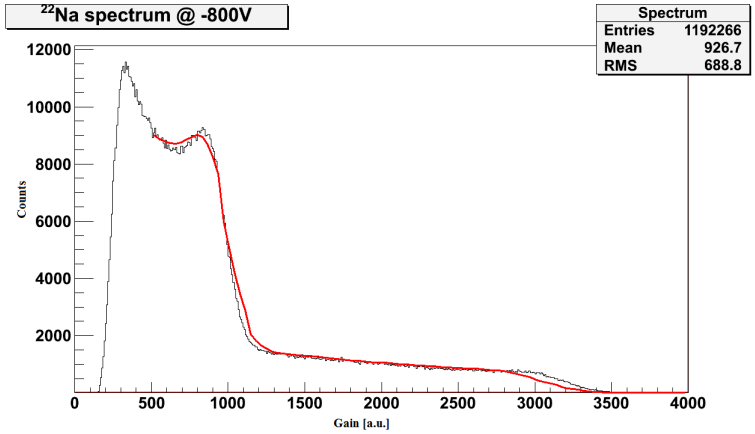

Figure 5: comparison between experimental data and simulated spectrum (red line).

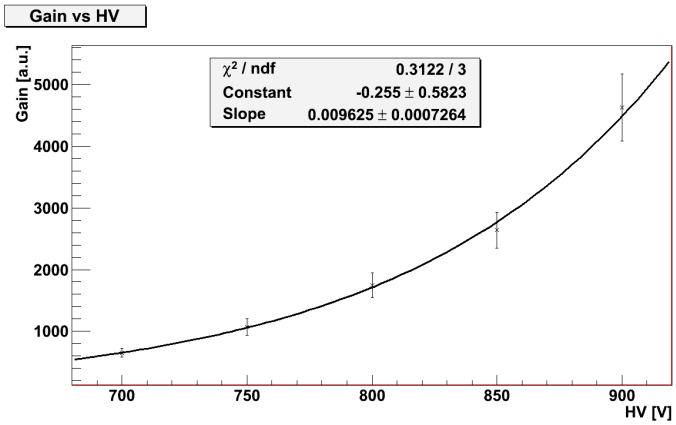

Figure 6: gain vs HV supply for 1.061 MeV peak.

3 PMT behaviour at high count rates

The expected count rate of the detector during high power JET operations is very high (order of 1MHz). Under these extreme conditions the PM tube can show a behaviour that deviates from the usual one at low count rates. This phenomenon can be studied to find corrections for gain deviations that can be applied to the acquired data.

For this purpose a LED pulse generator with adjustable pulse frequency can be used. The signal generated by the LED pulses is fed to the PMT and the resulting spectrum, that shows a monoenergetic peak, is analysed. Using different frequency values one can compare gain and resolution of the photomultiplier under different operational conditions.

3.1 Measurements

In figure 7 gain and resolution variations vs frequency of the LED generator are plotted. It is evident that there are significant variations for frequencies over 400kHz and that these are larger when a higher voltage is used. The resolution (fig.7(c)) doesn't show a clear tendency, while gain seems to decrease with frequency for 900, 850 and 800 volts supplies and slightly increase for 750 and 700 volts supplies. However it is important to note that when using the two highest values of the HV (900 and 850 volts) the pulses are distorted because of the saturation of the PMT, so these data are not reliable. The dependence of the LED peak position on the supplied high voltage of the photomultiplier is shown in figure 8 and still follows the law (1).

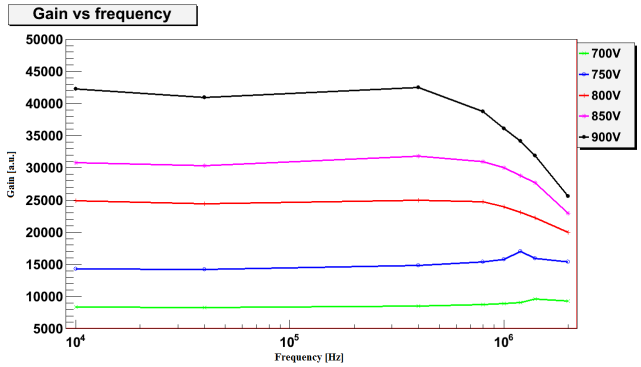

(a)

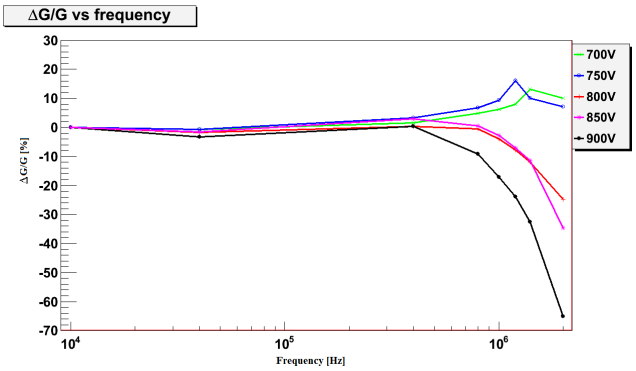

(b)

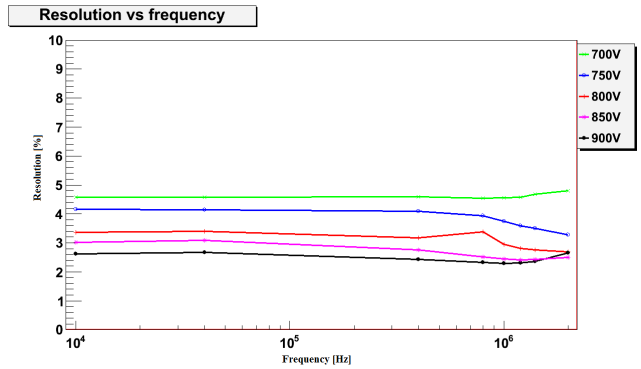

(c)

Figure 7: (a) gain vs frequency; (b) gain variation with reference to gain at 10kHz vs frequency; (c) resolution vs frequency.

4 ADC nonlinearity

Data acquisition is performed with a SP Devices ADQ214 digital card (table 3) that uses an Analog to Digital Converter (ADC) to convert analog signals into digital signals. The ADC has a voltage input range V_{pp}, which is divided into 2^n steps (codes), where n is an integer positive number called resolution. The $i-th$ code is activated when the voltage level in the input is between V_i and $V_i + W_i$. In principle the width W_i of each step should be always the same, i.e. $W_{IDEAL} = V_{pp}/2^n$, but a real ADC cannot have a perfectly linear response. However deviations from the ideal case can be measured and used to correct the collected data.

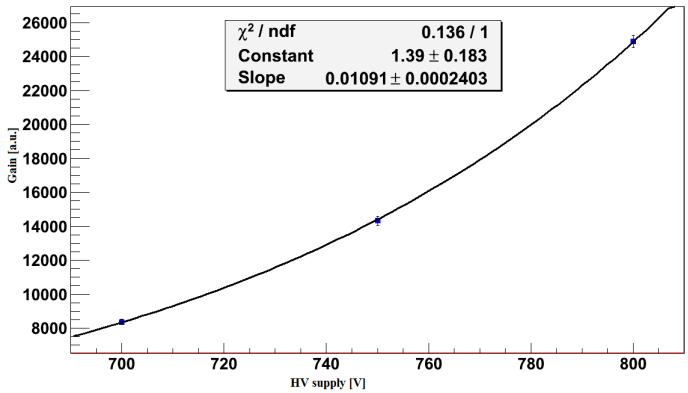

Figure 8: LED pulses gain vs HV supply.

Table 3: ADQ214 main features

Number of channels	2
ADC Resolution	14 bits
Sampling rate	$70 - 400$ MSPS
Input range	2.2 V_{PP}

A common method for this measurement is the histogram test. A triangular wave with amplitude that slightly exceeds the input range is fed to the ADC, so that the distribution of the number of times each code is activated should be uniform (except for the higher and the lower codes that are not taken into accout). The parameters that extimate the non linearity are the Differential Non Linearity (DNL) and the Integral Non Linearity (INL), which can be calculated using the formulas:

$$DNL(i) = \frac{COUNTS(i)}{EXPECTED} - 1 \tag{3a}$$

$$INL(i) = \sum_{n=1}^{i} DNL(n) \tag{3b}$$

where $COUNTS(i)$ is the number of counts of the $i-th$ code while $EXPECTED$ is the number of counts expected in each code assuming a uniform distribution and can be calculated simply dividing the total number of counts by the number of codes.

4.1 Measurements

DNL and INL graphs are shown in figure 9. The statistical error in the DNL for the i-th code is $\Delta DNL(i) = \sqrt{COUNTS(i)}/EXPECTED$. The average number of counts in each code is 21896, so $< \Delta DNL >= 0.0068$. From the DNL the transfer function of the ADC is obtained and can be used to correct the data acquired by the card. This means that the real voltage value associated with each code is computed using the formulas:

$$RESP(0) = V_{MIN} + \frac{W_{IDEAL}}{2} \tag{4a}$$

$$RESP(2^n - 1) = V_{MAX} - \frac{W_{IDEAL}}{2} \tag{4b}$$

$$RESP(i) = Resp(i-1) + W_{IDEAL} \cdot [DNL(i) + 1] \tag{4c}$$

An example of this correction is shown in figure 10. It's worth noting that even though the INL graph looks quite bad, the corrections needed (fig.10) are not huge. This is because they are relative (because of the baseline restoration, see 1.3), so what matters is the DNL, and it's clear from the graph 9(a) that the biggest non linearities are in the first codes (on the left) and to a lower degree in the last codes (on the right). Since the baseline level is situated around the central codes, large corrections will be needed only in case of very high pulses, when the first (negative pulses) or the last (positive pulses) codes come into play.

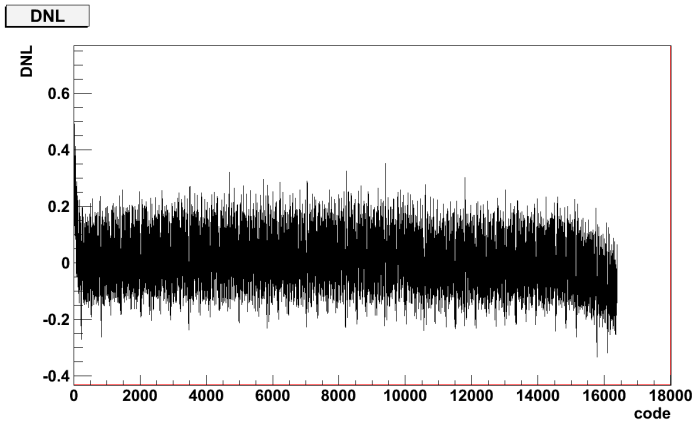

(a)

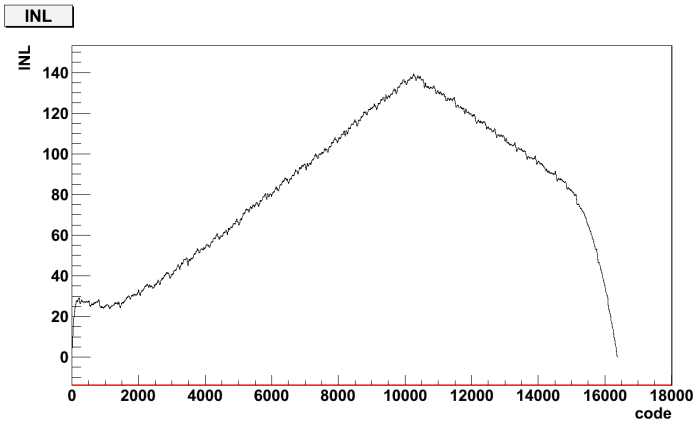

(b)

Figure 9: (a) Differential Non Linearity; (b) Integral Non Linearity.

5 Discussion and conclusions

The small dimensions of the detector give rise to an efficiency loss in the ^{22}Na spectrum that is visible at energies higher than 1 MeV. This is due to secondary electrons escape from the detector, so that their energy is not completly collected. The MCNP model allows to take this into account and to locate the correct position of the peak. We expect this effect to be smaller when dealing with neutron spectra because in this case the secondary particles, i.e. protons, have a shorter range in matter.

The study of the behaviour of the PMT with high frequency LED pulses has given some indication that the gain should vary when the count rate is higher than 400 kHz. While LED pulses are equally spaced in time, during JET operations neutron signals will be randomly distributed, so some study with this kind of events is needed in order to find the best possible correction.

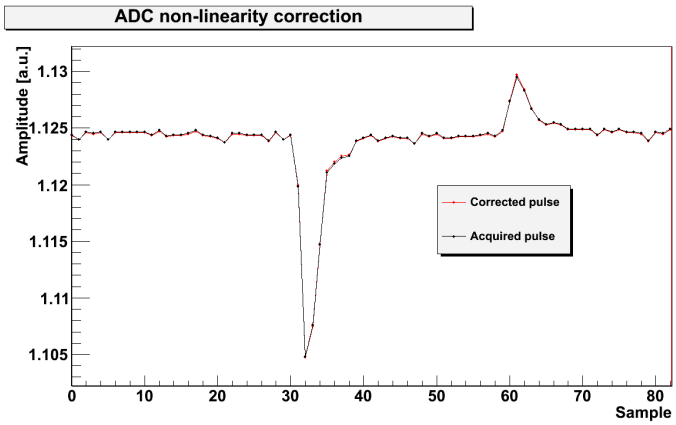

Figure 10: example of correction of a pulse.

The digitizer's ADC has shown some large nonlinearities that nevertheless are located in the lower codes. This means that for most of the pulses acquired the corrections for nonlinearity are not so important.

In conclusion the characterization of the detector presented in this report has shown that the NE-213 meets the requirements to be installed with the MPR on JET and used as intended. Moreover the LED pulse generator and the sodium source can give the corrections needed for the gain drift. Finally the acquired data will provide the JET neutron flux with higher time resolution than achieved so far.

References

[1] H. Sjöstrand et al., *Fusion Power Measurement Using a Combined Neutron Spectrometer-camera System at JET*, JET-EFDA, Culham Science Centre, OX14 3DB, Abingdon, United Kingdom (2009).

[2] G.F. Knoll, *Radiation Detection and Measurement*, Third edition, John Wiley & Sons, Inc. (2000).

[3] H.H. Knox and F.G. Miller, Nucl. Inst. and Meth. 101 (1972) 519.